African J. Biol. Sci., 18 (2): 199-224 (2022)
ISSN 1687-4870 **e- ISSN 2314-5501 (online)**
www.ajbs.journals.ekb.eg **E.mail: aasdjournal@yahoo.com**

The ameliorative influence of melatonin against hepatotoxicity-induced by taxol in adult rats

Hanaa R. Aboelwafa*, Ramadan A. Ramadan, and Faten M. Abdelhamid
Department of Biological and Geological Sciences, Faculty of Education,
Ain Shams University, Roxy, Cairo, Egypt
* Corresponding author E-mail: hanaarezk@edu.asu.edu.eg

Received: Nov. 28, 2022; Accepted: Dec. 15, 2022; Available online: Dec. 25, 2022

ABSTRACT

Cancer is a worldwide growing health problem caused expanding utilization of chemotherapy which is still the most popular and first-line method of treating malignancies. The current study aimed to use histological, histomorphometrical, immunohistochemical, and ultrastructural protocols to evaluate the hepatotoxic effect of Taxol (TXL) and the ameliorative influence of melatonin (MLT) against toxic impacts in the liver of adult rats. Fifty rats were used and randomly divided into four groups: control, sham, TXL (7.5 mg kg^{1} i.p.), MLT (10 mg kg^{-1} i.p.) and MLT+TXL (10 mg kg^{-1} + 7.5 mg kg^{-1} i.p.) groups. The results indicated the presence of numerous histopathological, histomorphometrical, and ultrastructural changes in the hepatic tissues of TXL-treated animals including destruction of the normal building of the hepatic lobules, with marked decline in the number of intact hepatocytes, and a rise in the number of necrotic hepatic cells, centrilobular and periportal inflammatory cells, and degraded Kupffer cells, in addition to noticeable apoptosis which was represented immunohistochemically by marked elevation in P53 and casapase3 (Cas3), and diminution in Bcl-2 immunoreactivities. Also, strong CD163 immunoreactivity was seen in TXL-treated rats. Nevertheless, co-administration of MLT with TXL reversed most of the histological and ultrastructural alterations triggered by TXL in rats. Moreover, MLT revealed a diminished effect against liver apoptosis and inflammation caused by TXL which was represented by elevation of immunoexpression of Bcl-2 and decreased immunoexpression of P53, Cas3, and CD163. In Conclusion, the present study proved that MLT has ameliorative impact against TXL-triggered hepatic toxicity through its antioxidant, anti-inflammatory and anti-apoptotic properties.

Keywords: Taxol, melatonin, liver, histopathology, immunohistochemistry, ultrastructure.

INTRODUCTION

One of the important classes of effective chemotherapy medications used is Taxanes (Paclitaxel / Taxol, Taxotere/ Docetaxel) and it is frequently applied to remedy major cancers such as thyroid, ovarian, breast, prostate, non-small cell lung, pancreatic, stomach, colon, bladder, neck, and head cancers (Lemstrova *et al.,* 2016; Hardin *et al.,* 2017).

Taxol (TXL) is one of the most potent anti-cancer medications (Marupudi *et al.,* 2007; Heinig *et al.,* 2013) and it is considered a mitotic agent that inhibits the vital functions of microtubules in mitosis by aggressively binding to their β-subunit of α/β-tubulin dimers, interrupting their dynamic, stabilizing their microtubule polymers, and ultimately inducing cell cycle arrest at the G2/M phase and eventual death (Fürst & Vollmar, 2013; Yang & Horwitz, 2017). A non-mitotic mechanism of TXL is supported by Smith *et al.* (2021) and Smith and Xu (2021) who explained that the stiff microtubules caused by paclitaxel act as a physical force to cause the tumor nucleus to break into many micronuclei. On the other hand, TXL can induce serious side effects like hypersensitive responses, endothelial dysfunction, neuropathy, cardiotoxicity, and hepatotoxicity, which reduce its notable efficiency (Serizawa *et al.*, 2012; Malekinejad *et al.,* 2017).

Melatonin (MLT) is a naturally occurring indoleamine (N-acetyl-5-methoxy tryptamine) that controls circadian rhythm, sleep, and mood (Reiter *et al.,* 2017). Organs containing MLT-related enzymes and cells expressing MLT receptors were likewise widely distributed (Hardeland *et al.,* 2011; Chen *et al.,* 2015). The powerful antioxidant, free radical scavenger, cell-modulating, anti-ischemic and anti-aging characteristics of MLT (Zhang *et al.,* 2017) changed its status from a hormone exclusive to the brain to that of an all-encompassing molecule controlling a wide range of biological processes, including reproductive cycles, energy balance, neuro-endocrine, cardiovascular, and immunological activity (Yu *et al.,* 2016; Ren *et al.,* 2017; Luo *et al.,* 2019). Also, the impact of MLT as an oncostatic agent with antitumor influence in various types of cancers have been recorded, including colorectal (Chok *et al.,* 2019), pancreatic (Tamtaji *et al.,* 2019), breast (Kong *et al.,* 2020), urological (Mehrzadi *et al.,* 2020), kidney (Maleki Dana *et al.,* 2020), gynecologic (Dana *et al.,* 2020), and cerebral (Pourhanifeh *et al.,* 2021) cancers. MLT`s antitumor effects vary and are associated with anti-inflammatory (Plaimee *et al.,* 2014), antioxidant (Alonso-González *et al*., 2018), anti-proliferative (Oshiba *et al.,* 2021) and apoptosis regulation (Samei *et al.,* 2021). Based on clinical observations of the improved effectiveness of chemotherapy associated with its usage, fewer side effects, and improved patient quality of life, MLT is being studied as a substance connected to the regulation of cancer development.

There were few studies on the effect of TXL on the hepatic tissues of mammals from the histological, histomorphometrical, immunohistochemical, and ultra-structural point of view. Therefore, the present investigation was designed to assess and evaluate the toxic consequences of TXL on the liver of adult rats and the possible attenuated effects of MLT against such harmful influences.

MATERIALS AND METHODS

Experimental animals

Fifty adult male Wistar rats *Rattus norvegicus* (16 to 18 weeks old and 250 and 300g weight) were obtained from Theodor Bilharz Research Institute, El-Giza, Egypt. Rats were housed in spotless plastic boxes that were supported by timber shavings, and they were eaten traditional food of rodent pellet diet along with unlimited amounts of water and milk. The rats were preserved in sterile environment with a 12-h light/dark cycle, at 25°C temperature, and a relative humidity of 55%. Prior to the trial, all rats were left for two weeks to adapt. The current experiment was carried out in line with the Institutional Animal Ethics/Committee of Ain Shams University's Approved Rules for Animal Research.

Pharmacological materials

TXL is a clear, colorless to slightly yellow viscous solution produced by Bristol-Myers Squibb Company Princeton NJ 08543 USA. MLT (item number Q20D023) was purchased as a powder from Sigma–Aldrich Chemie GmbH (Taufkirchen, Germany). All other chemicals used in the current study were of analytical grade and Merck quality.

Experimental design

The rats were evenly allocated into five experimental groups, each with 10 animals. Rats in control group received physiological saline solution every day for 30 days; rats in sham group were intraperitoneally (i.p.) injected with physiological saline and absolute ethanol with a final concentration under 0.1% daily for 30 days; animals in TXL-treated group were i.p. injected with TXL at a dose equivalent to 7.5 mg kg^{-1} weekly at days 0, 7, 14, 21 and 28 in line with Ozcelik *et al.* (2010)

and Malekinejad *et al.* (2015 & 2017); rats in MLT-treated group were daily i.p. injected for 30 days with 10 mg kg^{-1} MLT which was freshly dissolved in a smaller quantity of 100% ethanol (0.5 mL) before diluted with physiological saline to the required concentration (10 mg kg^{-1}) with the ethanol's final concentration was under 0.1%. The dose and preparation of MLT were determined according to Ghasemi *et al*. (2010) and Hashish & Elgaml (2016); and the rats of MLT+TXL-treated group were treated with MLT (10 mg kg^{-1}, daily) alongside with TXL (7.5 mg kg^{-1}, weekly). At the end of each experiment, all rats were starved of food for the entire night before being anesthetized with diethyl ether, thoroughly dissected, and the liver was extracted, quickly washed with normal saline solution, and processed for further histological, immunohistochemical, and ultrastructural techniques.

Histological preparation

Liver samples from control and other treated animals were cut off into small pieces that were fixed for 24 h in aqueous Bouin's fixative before being subjected to the standard paraffin sectioning procedures described by Bancroft and Gamble (2002). Ehrlich's hematoxylin and eosin (H&E) was utilized for staining the sectioned paraffin slices of 4-6 µm thick, which were subsequently cleared in xylene, mounted in DPX, examined, and captured with BX-40 Olympus compound light microscope provided with a Panasonic CD-220 camera.

Histomorphometrical measurements

The numbers of intact and necrotic hepatocytes, degraded Kupffer cells, infiltrated inflammatory cells in the centrilobular and in the periportal areas were counted in five random samples from each group using computed image analysis system (Leica Qwin, 500 Software, Germany) at Oral & Dental Pathology Department, Faculty of Dental Medicine for Girls, Al-Azhar University.

Immunohistochemical preparation

The Avidin Biotin Complex (ABC) method was used for the immunohistochemical estimation of the immunoexpression of the reactive proteins Bcl-2, P53, caspase3 (Cas3), and CD163 (Kiernan, 2015). In brief, deparaffinized 5µm-thick buffered neutral formalin-fixed sections were rehydrated, rinsed in phosphate-buffered saline (PBS) for 10 min, and then in 3% hydrogen peroxide to prevent endogenous peroxidase activity. Afterwards, these sections were incubated for 1–2 h at room temperature with the appropriate dilution of the primary antibodies that were illustrated in Table (1), then kept at 4ºC overnight in a refrigerator. After that, the tissue slices were washed 5 times in PBS, incubated for 10 min with biotinylated goat anti-polyvalent, subsequently they were incubated for 1 h with ABC, then they were rinsed in PBS, incubated for 7–9 min in diaminobenzidine tetrahydrochloride (pH 7.2) with 10 ml H_2O_2 sequenced by 4 changes of PBS. Instantly, the tissue slices were counterstained for 2 min with Mayer's hematoxylin, washed in tap water, dehydrated, cleared, and covered with cover slips. Every time, negative controls were stained using the standard immunostaining procedure, but PBS was used in place of the primary antibody. In accordance with the guidelines and suggestions of the manufacturer (Thermo Fisher Scientific USA), the reagents and antibodies were accurately used.

Table (1). Antibodies employed in immunohistochemical evaluation.

Antibody	**Bcl-2**	**P53**	**Cas3**	**CD163**
Code	MA5-11757	MA5-12557	MA5-11516	MA5-11458
Clone	100/D5	DO-7	3CSP01 (7.1.44)	10D6
Antigen retrieval	PBS, pH 7.4 with 0.2% BSA	PBS, pH 7.4	PBS, pH 7.4 with 0.2% BSA	Tissue culture supernatant
Dilution	1:50	1:100-1:200	1:50-1:100	1:25-1:50
Source	Mouse/IgG, kappa	Mouse/IgG2, kappa	Mouse/IgG2a	Mouse / IgG1

Image analysis of immuno-histochemical markers

The immunostained sections were initially examined and captured using a compound light microscope equipped with a Leica Qwin 500 Software computed image analysis system (Germany) to evaluate the number of positive cells and the location of immunostaining inside these cells. If there was membranous and/or cytoplasmic brown staining, the cells were considered positive. At the Department of Oral and Dental Pathology, Faculty of Dental Medicine for Girls, Al-Azhar University, the immunoreactivity of Bcl-2, P53, Cas3, and CD163 reactive proteins were estimated by calculating the area proportion of the positive immunostained cells comparative to the total number of the examined cells for each field at x200 magnification, with a measuring frame of an area of 11434.9 mm^2/5 fields. To begin with, the image analyzer was automatically calibrated to change the measurement units (pixels) generated by the image analyzer application into real micrometer units. For statistical purposes, the mean percentage of immunostained cells for all tissue sections in each experimental group was determined.

Ultrastructural preparation

Freshly removed livers of all experimental groups were divided into tiny segments and forthwith fixed for 24 h in cold 4F1G (4% formalin plus 1% glutaraldehyde at pH 2.2), followed by post-fixation in 1% phosphate buffered osmium tetroxide (pH 7.3) for 2-4 h (Dykstra *et al*., 2002), then the specimens were processed for transmission electron microscopy (TEM) for ultrastructural analysis after fixation. Finally, the stained grids were analyzed and captured by camera using a JEOL.JEM-1200-EX-Electron microscope at the Faculty of Agriculture, Cairo University's Central Laboratory.

Statistical analysis

Results were introduced as mean ± SEM. By using the one-way analysis of variance (ANOVA) and the SPSS/17.0 statistical software, differences between animal groups were determined. By using the Tukey's multiple comparison Post hoc test, statistical significances between groups were evaluated, and statistical significance was defined as *p* values of 0.05 or less.

RESULTS

Histological results

The examination of sections of liver from control (Fig. 1A&B) and sham (Fig. 1C&D) rats showed normal parenchymal structure of the liver tissues in the centrilobular and periportal areas including well-extended hepatic strands appeared radiated around intact central veins and throughout the portal tracts which were made up of typical hepatic portal veins, hepatic portal arteries and bile ductules. In addition, intact Kupffer and endothelial cells were seen lining the typical blood sinusoids located in-between the hepatic strands.

TXL-treated rats' hepatic tissues were displayed significant histological alterations in the centrilobular (Fig. 1E) and the periportal (Fig. 1F) areas, where the hepatic lobules lost their normal configuration and most hepatocytes appeared degenerated with vacuolated cytoplasm and with rather deformed nuclei showing pyknotic or karyorrhectic manifestation. Also, the blood vessels including the central veins, hepatic portal veins and hepatic portal arteries appeared severely devastated being dilated and badly blocked with stagnant hemolyzed blood, besides, the inflammatory cells were observed to infiltrate the area near their borders. The lining endothelium of these blood vessels seemed eroded and degraded in certain places. In addition, the hepatic sinusoids displayed devastation, congestion, and lined with large activated phagocytic Kupffer cells that seemed to be detached from their borders.

Nevertheless, MLT-treated rats displayed marked improvement of the hepatic architecture in the centrilobular (Fig. 1G) and periportal (Fig. 1H) areas similar to the control and sham groups. Otherwise, the histological structure of the hepatic tissues of MLT+TXL treated rats showed outstanding refinement in the centrilobular (Fig. 1I) and periportal (Fig. 1J) zones where most hepatocytes and blood sinusoids looking regular. Additionally, the blood vessels including the central veins, hepatic portal veins, and hepatic portal arteries appeared restoring their regular architecture.

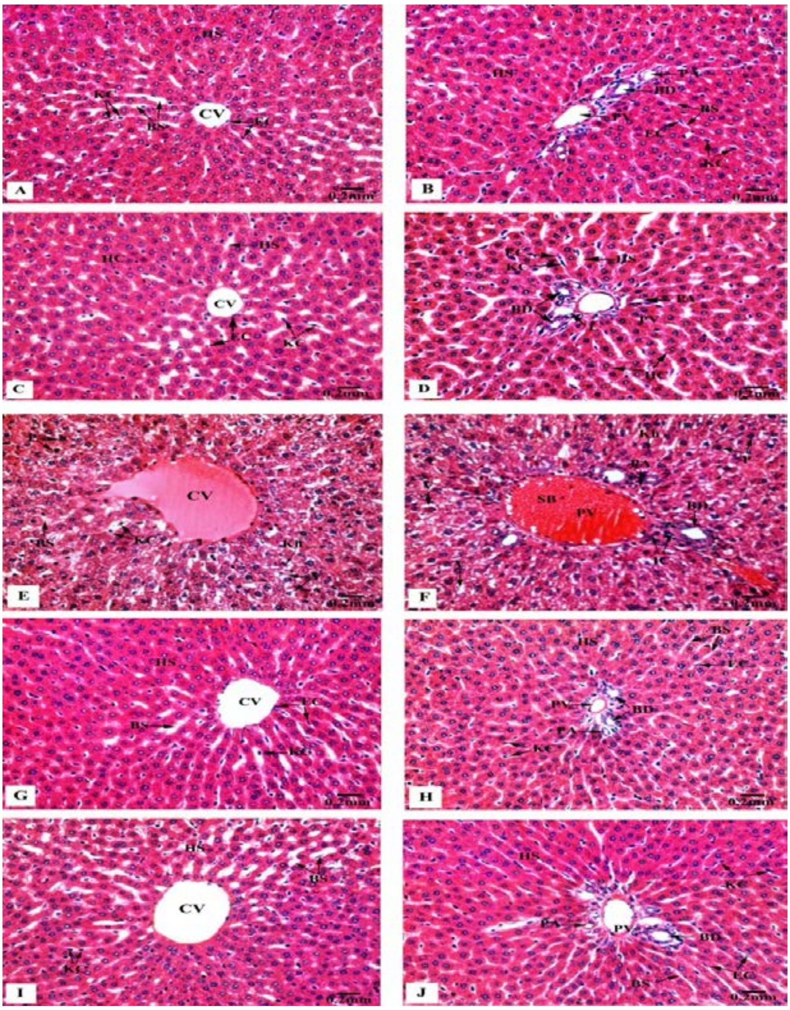

Fig. (1). Hematoxylin and eosin (H&E)-stained liver sections obtained from the control and treated animal groups demonstrating **(A&B)** well-organized hepatic strands (HS) separated by regular blood sinusoids (BS) that are lined with intact endothelial (EC) and Kupffer (KC) cells in both hepatic zones; the centrilobular zone which characterized with the presence of narrowed central vein (CV) appeared with regular boundaries and lined with endothelial cells (EC), and the periportal zone that composed of well-structured hepatic portal vein (PV), hepatic portal artery (PA), and bile ductule (BD) in control rats; **(C&D)** regular histological characteristics of the hepatic tissue architecture in both the centrilobular and periportal areas in sham rats; **(E&F)** deteriorated hepatocytes separated by destructed hepatic blood sinusoids (BS) appeared lined with more rounded Kupffer cells (KC) being pushed into the lumens, and most of these hepatic cells showed cytoplasmic vacuolation (V) and nuclear pyknosis (P) or karyorrhexis (Kh) in both zones; the centrilobular and periportal zones. Additionally the central vein (CV), portal vein (PV) and portal artery (PA) were widened and congested with stagnant blood (SB), besides infiltrated inflammatory cells (IC) are also seen in TXL-treated rats; **(G&H)** typical centrilobular and periportal hepatic structure resembling that of the control rats was seen in MLT-treated rats; **(I&J)** a noticeable improvement in the centrilobular and periportal regions of the hepatic tissues' histological structure in rats receiving MLT + TXL treatment.

Histomorphometrical results

It was obvious from Table (2) that the liver tissues of TXL-treated rats revealed a highly significant fall ($p \leq 0.001$) in the number of intact hepatic cells (-59.6% change), and a highly significant elevation ($p \leq 0.001$) in the number of necrotic hepatic cells (1150% change), centrilobular inflammatory cells (704.6% change), periportal inflammatory cells (329.8%), and degraded Kupffer cells (574% change) in comparison with control animals.

Whereas, concomitant treatment with MLT ameliorated these impaired hepatic parameters which were observed in TXL-intoxicated rats where moderately significant rise ($p \leq 0.05$) was estimated in the number of necrotic hepatocytes (503% change), a non-significant elevation ($p \leq 0.05$) in the number of devastated Kupffer cells (126% change), centrilobular inflammatory cells (284.6%), and periportal inflammatory cells (148.8% change) of the examined hepatic tissues, with the number of normal hepatocytes (-26.9% change) illustrated a non-significant decline ($p \geq 0.05$) in comparable with those of control rats.

Examination of hepatic tissues of sham and MLT-treated groups demonstrated a non-significant decline ($p \geq 0.05$) in the number of normal hepatocytes (-1.92% , -3.84% change, respectively), and a non-significant elevation ($p \geq 0.05$) in the number of necrotic hepatocytes (10%, 53.3% change, respectively), deteriorated Kupffer cells (4%, 8% change, respectively), centrilobular inflammatory cells (3%, 138.4% change, respectively), and periportal inflammatory cells (15.8%, 69% change, respectively) as illustrated in Table (2).

Table 2. Histomorphometrical analysis of hepatic parameters of control and treated animal groups.

Hepatic Parameters	Animal Groups				
	Control	**Sham**	**TXL**	**MLT**	**MLT+TXL**
No. normal hepatocytes	260±1.70[a]	255±2.56[a]	105±1.77[b]	250±3.88[a]	190 ± 3.50[a]
No. necrotic hepatocytes	12±1.02[a]	13.2±1.5[a]	150±3.09[b]	18.4±0.93[a]	72.2±1.69[c]
No. inflammatory cells in centrilobular zones	6.5±1.33[a]	6.7±1.64[a]	52.3±2.66[b]	15.5±1.83[a]	25 ±2.05[a]
No. inflammatory cells in periportal zones	44.2±1.33[a]	51.2±1.64[a]	190±3.66[b]	74.7±1.83[a]	110±2.05[a]
No. deteriorated Kupffer cells	10±1.52[a]	10.4±1.86[a]	67.40±2.66[b]	10.8±1.16[a]	22.6±1.96[a]

Data are introduced as Mean ± SEM (n = 5 for each group). Means present in the same row and having diverse superscripts differ significantly at 5 % ($p \leq 0.05$) level of significance according to ANOVA test. TXL: Taxol; MLT: Melatonin.

Immunohistochemical results

Bcl-2 immunoreactivity

TXL-intoxicated rats illustrated a weak Bcl-2 immunostainability (Fig. 2D) compared to the hepatic tissues obtained from control (Fig. 2B), sham (Fig. 2C) and MLT-treated (Fig. 2E) rats which showed strong Bcl-2 immunoreactivity. Concomitant treatment of rats with MLT and TXL up-regulated the immunoexpression of Bcl-2 as seen in Figure (2F). Negative control sample revealed non-stainability (Fig. 2A).

As shown in Table (3), sham and MLT-treated groups exhibit a non-significant decrease ($p>0.05$) in the area percentage of Bcl-2 immunoexpression (-0.24% and -5.92% change, respectively) in comparable with the value of control rat group. Meanwhile, a highly significant reduction ($p \leq 0.001$) was estimated for the area percentage of Bcl-2 immunoexpression in TXL-treated group (-65.04% change) when compared with the control group, but a non-significant decline ($p>0.05$) was recorded in MLT+TXL-intoxicated group (-25.18% change) related to the control value.

P53 immunoreactivity

Liver tissues of control (Fig. 3B), sham (Fig. 3C) and MLT-treated (Fig. 3E) animal groups manifested mild P53 immunostainability, while the rats intoxicated with TXL demonstrated a strong P53 immunostaining (Fig. 3D). MLT+TXL co-administered animals showed weak P53 immunoreaction (Fig. 3F). A negative stainability was found in negative control sample (Fig. 3A). Immunohistochemical quantitative analysis of the reactive protein P53 manifested that the liver tissues of sham and MLT-treated rat groups had a non-significant rise ($p>0.05$) in P53 immunoexpression`s area percentage (1.62% and 10.52% change, respectively) compared with that of control group. But a highly significant increase ($p\leq0.001$) was recorded in TXL-treated group (278.2% change) relative to control value. Alteration of the immunoexpression of P53 reactive protein was seen in the examined tissues of rats` liver treated with MLT alongside with TXL, where a non-considerable increase ($p>0.05$) was recorded (20.9% change) compared to control group (Table 3).

Cas3 immunoreactivity

Control (Fig. 4B) and sham (Fig. 4C) rat groups exhibited weak Cas3 immunostainability in their hepatic tissues. Similarly, MLT-treated rats manifested a weak immunostaining for Cas3 (Fig. 4E). Conversely, liver tissues of TXL-treated rats illustrated strong Cas3 immunostaining (Fig. 4D). MLT co-administered with TXL-treated groups illustrated moderate Cas3 immunoreactivity (Fig. 4F). No reaction was seen in the negative control liver tissues (Fig. 4A). As noticed in Table (3), a highly significant rise ($p\leq0.001$) in the immunoexpression of Cas3 reactive protein was assessed for TXL-treated group (121.395% change) in comparison with control group. In the meantime, modulation of the immunoexpression of Cas3 reactive protein was seen in the examined hepatic tissues of rats treated with MLT alongside with TXL, where a non-significant rise ($p>0.05$) was observed (21.39% change) relative to control ones. A non-significant increase ($p>0.05$) was also recorded for the area percentage of Cas3 immunoexpression in sham and MLT-treated rats (1.86 % and 4.18 % change, respectively) relative to control rats.

CD163 immunoreactivity

The hepatic tissues from control (Fig. 5B), sham (Fig. 5C) and MLT-treated (Fig. 5E) animal groups showed poor CD163 immunostaining, whilst the hepatic sections of TXL-treated animals (Fig. 5D) showed strong CD163 immunostainability. On the other side, the hepatic tissues of rats from MLT co-administered with TXL (Fig. 5F) illustrated mild CD163 immunoreactivity compared with TXL-treated rats. Figure (5A) showed no staining in negative control hepatic tissues. Table (3) revealed that a highly significant elevation ($p\leq0.001$) in the immuno-expression of CD163 reactive protein was assessed in liver tissues of TXL-treated rats (207.74% change) when compared with the data of control rats. Meanwhile, a non-significant increase ($p>0.05$) in CD163 immunoexpression was estimated for both sham and MLT-treated rat groups (4.07% and 14.98% change, respectively) compared to control group. A non-significant increase ($p>0.05$) was evaluated for CD163 immunoexpression in MLT+TXL treated group (49.95% change) in comparison with those of control rats.

Table (3). Immunohistochemical quantitative analysis of Bcl-2, P53, Cas3 and CD163 expressions in hepatic tissues of control and treated rat groups.

Immunohisto-chemical Parameters	Experimental Groups				
	Control	Sham	TXL	MLT	MLT + TXL
Bcl-2	24.66±1.93[a]	24.60±1.90[a]	8.62±1.39[b]	23.20±.99[a]	18.45±1.75[a]
P53	10.45±1.37[a]	10.62±1.00[a]	39.53±2.45[b]	11.55±.74[a]	12.55±1.90[a]
Cas3	21.5±1.22[a]	21.9±1.2[a]	47.61±2.25[b]	22.4±1.25[a]	26.11±1.7[a]
CD163	9.81±1.18[a]	10.21±1.10[a]	30.19±1.26[b]	11.28±1.50[a]	14.71±1.17[a]

Data are introduced as Mean ± SEM (n = 5 for each group). Means present in the same row and having diverse superscripts differ significantly at 5% ($p \leq 0.05$) level of significance according to ANOVA test. TXL: Taxol; MLT: Melatonin.

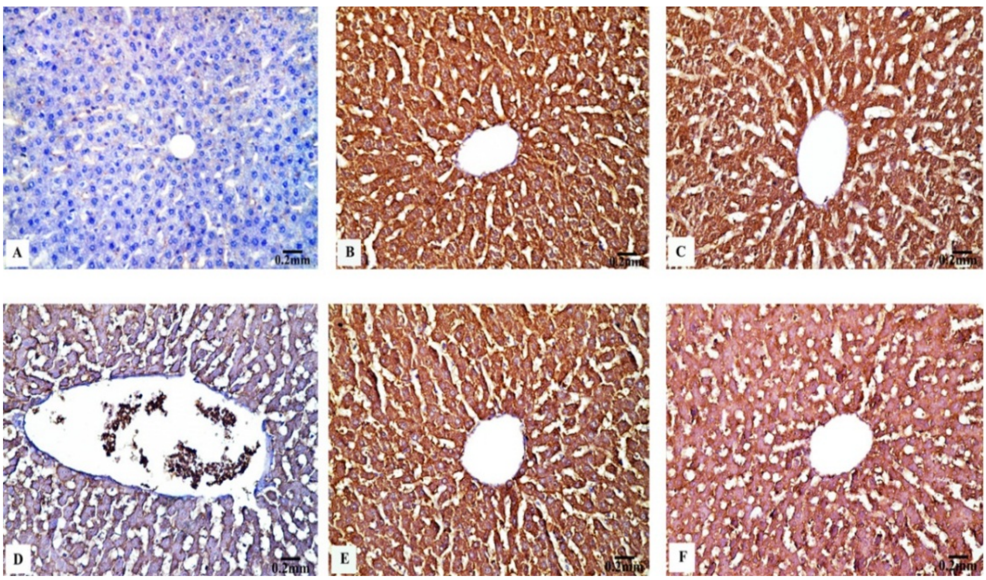

Fig. (2). Immunohistochemical expression of Bcl-2 in hepatic tissues of control and treated rats illustrating **(A)** a negative staining in negative control; **(B&C)** a strong stainability in control and sham groups, respectively; **(D)** a weak stainability in TXL-treated group; **(E)** a strong reactivity in MLT-treated group; **(F)** a moderate immunostaining in MLT+TXL -treated group.

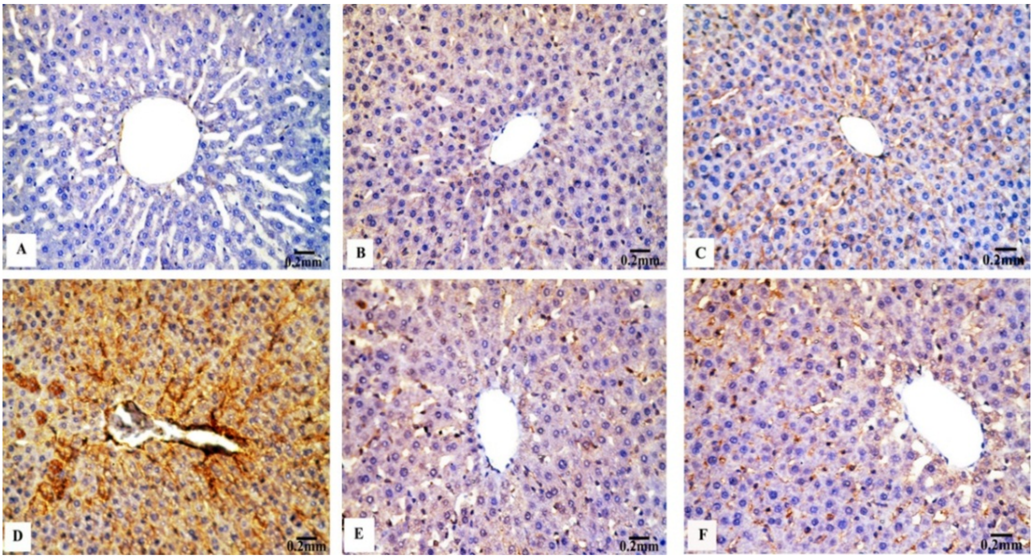

Fig. (3). Immunohistochemical expression of P53 in hepatic tissues of control and treated rats revealing **(A)** no staining in negative control; **(B&C)** a poor immunostainability in control and sham groups, respectively; **(D)** a strong immunoreaction in TXL-treated group; **(E)** a mild immunoreactivity in MLT-treated group; **(F)** a moderate immunoreactivity in MLT + TXL-treated group.

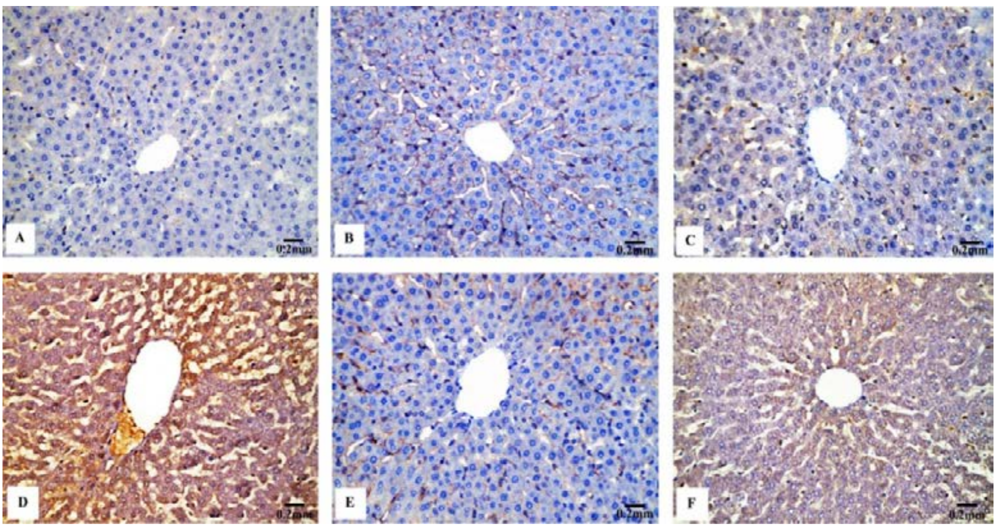

Fig. (4). Immunohistochemical expression of Caspase-3 in hepatic tissues of control and treated rats showing **(A)** a passive stainability in negative control; **(B&C)** a poor immunostainability in control and sham groups, respectively; **(D)** an intense immunostainability in TXL-treated group; **(E)** a weak immunostainability in MLT-treated group; **(F)** a modest immunoreaction in MLT + TXL-treated group.

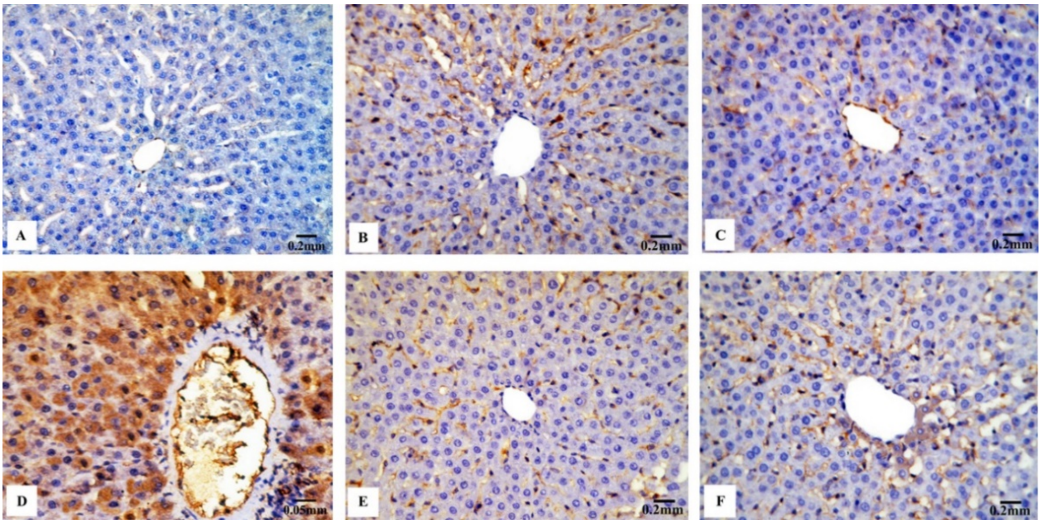

Fig. (5). Immunohistochemical expression of CD163 in hepatic tissues of control and treated rats showing **(A)** no immunostainability in negative sample; **(B&C)** a poor immunoreactivity in control and sham rats, respectively; **(D)** a strong immunostainability in TXL-treated group; **(E)** mild immunostainability in MLT-treated group; **(F)** a weak immunostainability in MLT + TXL-treated group.

Ultrastructural results

The hepatic cells of control (Fig. 6A) and sham (Fig. 6C) rat groups showed regular fine structure, where the cytoplasm contained much scattered rounded or elongated mitochondria having short transverse cristae and medium electron-dense matrices, rough endoplasmic reticulum composed of thin paralleled cisternae, smooth endoplasmic reticulum formed of clusters of tiny rods and vesicles and few electron-dense lysosomes. Each hepatocyte had one or occasionally two spherical nuclei having electron dense nucleoli, dense peripheral heterochromatin, dispersed granules of euchromatin and bordered by distinguished nuclear envelopes. Also, normal blood sinusoids having intact attached Kupffer cells and appeared separated from the neighboring hepatocyte by the space of Disse that appeared narrow with extended microvilli are clearly displayed in control (Fig. 6B) and in sham (Fig. 6D) rat groups.

However, the hepatocytes of TXL-intoxicated rats manifested severe fine structural alterations as represented in Figure (6E-G). The cytoplasm appeared with proliferated electron-dense cisternae of rough endoplasmic reticulum, as well as destructed cisternae of both types of endoplasmic reticula, mitochondria showed weak electron-dense matrix and brokendown and loss of cristae, lysosomes, few lipid droplets, and cytoplasmic vacuoles. The nuclei of some hepatocytes showed hardly distinct nuclear envelopes and chromatin dissolution (Fig. 6E&F), while the others exhibited signs of pyknosis (Fig. 6G). Dilated blood sinusoid with deteriorated Kupffer cell having electron-dense nucleus is also observed (Fig. 6H).

As revealed in Figure (6I), hepatocytes of MLT-treated rats revealed the same ultrastructural features of the control rats, where they appeared packed with regular mitochondria, rough and smooth endoplasmic reticula, and lysosomes. Besides, their nuclei appeared rounded with normal structural organization. Figure (6J) revealed well-structured blood sinusoid with intact Kupffer cells, and space of Disse separating the neighboring hepatocytes.

Electron micrographs of the hepatocytes of rats co-treated with MLT and TXL (Fig. 6K) entirely confirmed the results performed in the histological section, where these cells appeared with nearly regular fine structural organelles, including the nuclei, endoplasmic reticula, mitochondria, and lysosomes. Besides, the blood sinusoids, Kupffer cells and space of Disse distinctly showed rather normal in appearance (Fig. 6L).

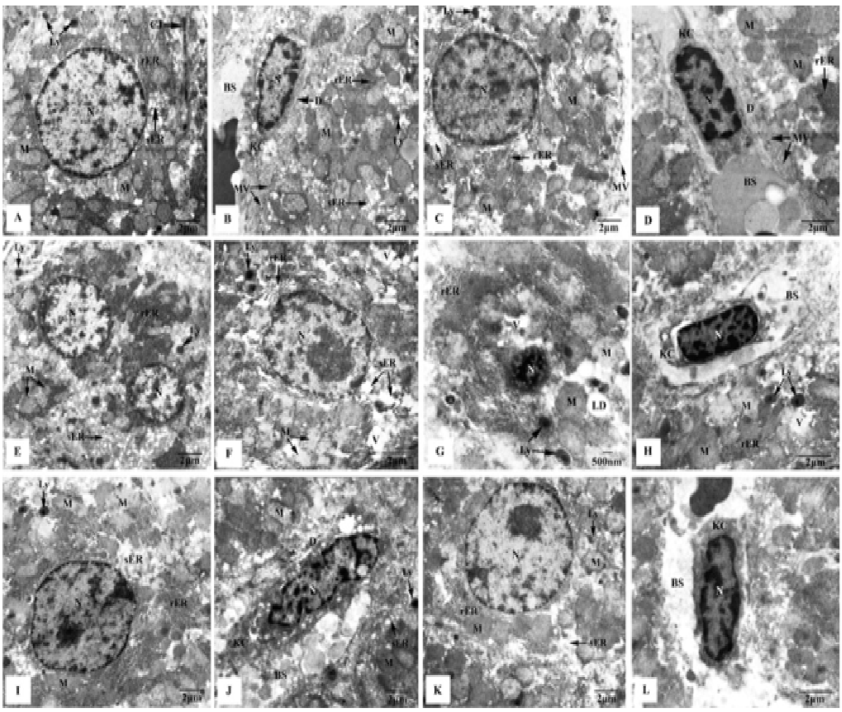

Fig. (6). Electron micrographs of liver tissues of control and treated rats showing **(A&B)** a hepatocyte with normal fine structural organization where it possesses an intact plasma membrane with cell junction (CJ), a nucleus (N), cytoplasm appeared crowded with mitochondria (M), lysosomes (Ly), rough (RER) and smooth (SER) endoplasmic reticula. Additionally, normal blood sinusoid (BS) with attached Kupffer cell (KC) leaving narrow space of Disse (D) with intact microvilli (MV) is seen in control rat; **(C&D)** a regular structural architecture is observed in hepatocyte and Kupffer cell (KC) in sham rat; **(E-H)** severe deterioration of the fine structure of the hepatocytes which appeared with degenerated cytoplasm displaying aggregation of density profiles of rough (RER) and smooth (SER) endoplasmic reticula, damaged mitochondria (M) with weak electron-dense matrix and lost their cristae, cytoplasmic vacuoles (V), lysosomes (Ly) and few lipid droplets (LD), in addition to nuclei with clear signs of pyknosis and karyorrhexis in TXL-treated rats. Dilated blood sinusoid (BS) with rounded Kupffer cells (KC) having electron dense nucleus (N) is also noticed; **(I&J)** an intact nucleus (N) and cytoplasm possessing mitochondria (M), lysosomes (Ly), rough (RER) and smooth (SER) endoplasmic reticula in hepatocyte of MLT-treated rat. Also, blood sinusoid (BS) with well-structured Kupffer cell (KC), as well as space of Disse (D) is revealed; (**K&L)** improvement of most of the cellular organization of hepatocyte which appeared with nearly normal nucleus (N), mitochondria (M), lysosomes (Ly), rough (RER), and smooth (SER) endoplasmic reticula, in addition to intact Kupffer cell (KC) lined the blood sinusoid (BS) of MLT+TXL-treated rat

DISCUSSION

Chemotherapy is particularly efficacious at preventing the spread of cancer cells (Bray *et al*., 2018) and Taxol (TXL) is considered one of the highly effective drugs used in the world which acts as anti-microtubule agents and possesses two unique properties including its ability to attach to a distinct binding site on the microtubule polymer and the ability to polymerize tubulin without the aid of co-factors (Ghafouri-Fard, *et al*., 2021). Consequently, it is vastly utilized to treat a variety of malignancies including lung, thyroid, prostate, breast, ovarian, head, and neck, in addition to Kaposi sarcoma (Lemstrova *et al.*, 2016; Hardin *et al.*, 2017). Despite TXL's advantages in the treatment of cancer cells, it has a lot of adverse effects on other human organs, particularly the liver, which is a key organ in the body's detoxification process for all medications and pollutants (Ozougwu, 2017).

The results of the present investigation showed that TXL administration caused varied histopathological and histomorphometrical alterations reflecting its hepatotoxic effect on the liver of the treated rats, including hepatocellular degeneration, hepatocytic necrosis/apoptosis, lymphocytic infiltration, dilation of sinusoidal spaces and dilatation/ congestion of blood vessels. In addition, TXL significantly decreased the number of normal hepatic cells, and markedly increased the numbers of necrotic hepatocytes, degraded Kupffer cells, and inflammatory cells, which are the most striking symptoms of structural damage of the liver. This study's findings are in line with those given by Palipoch *et al.* (2014) following the administration of cisplatin, Shokrzadeh *et al.* (2014) after cyclophosphamide application, Chaudhary *et al.* (2016) post doxorubicin treatment, and Khorwal *et al.* (2017) post cyclophosphamide intoxication into rats.

The existing findings showed that most hepatocytes of TXL-treated rats illustrated severe degradation marked by signs of necrosis. These degenerative changes could be linked to the discharge of lysosomal enzymes, and to the disturbance of the functions of hepatocytes, leading to a massive flowing of water and sodium ions, causing cytoplasmic disintegration (Del Monte, 2005). Different anti-cancer drugs are well known medication causing necrosis such as cyclophosphamide (Khorwal *et al.,* (2017), TXL (Malekinejad *et al.,* 2017) and cisplatin (Hassan *et al.,* 2021).

Additionally, the hepatic tissues obtained from TXL-treated rats revealed marked elevation in the number of degraded Kupffer cells. These cells are tissue-resident macrophages which can move along hepatic sinusoidal endothelial cells and ingest foreign pathogens and apoptotic cells that are entered into the liver through the portal venous system (Sato *et al.,* 2016).

Furthermore, the hepatic tissues of TXL-intoxicated rats exhibited significant rise in the number of infiltrated inflammatory cells, confirming that TXL react with the interstitial hepatic tissues, resulting in different immunological reactions (Johar *et al.,* 2004). Similar observations were also obtained by Ahmed and Ghobara, (2013) following cisplatin administration, and Khorwal *et al.* (2017) post cyclophosphamide treatment.

The current investigation showed cytoplasmic vacuolation of the hepatocytes after TXL treatment. This harmful effect is thought to be a manifestation of necrosis, which was found in many mammalian cells after exposure to various drugs treatment (Huang *et al.,* 2020; Hassan *et al.,* 2021). Furthermore, noticeable dilation and congestions of the hepatic vasculatures recorded in the liver sections of TXL- treated rats might be resulted from obstruction of these vessels as mentioned by Shokrzadeh *et al.* (2014) in rats treated with cyclophosphamide.

The immunohistochemical results demonstrated that TXL administration to rats caused hepatic apoptosis which was proved by a marked decline in the immunoexpression of Bcl-2 and a considerable elevation in the immunoexpression of P53 and Cas3 in the hepatic tissues. The anti-apoptotic Bc1-2 protein is crucial for cell survival and apoptosis regulation. It participates in P53 apoptotic path, and the interaction of these proteins must be balanced for an organism to be susceptible to apoptosis (Tzifi *et al.,* 2012). P53 is a transcription factor which controls transcription rate for numerous genes included in DNA repair, cell cycle regulation, and apoptosis. If the damage cannot be healed, expressed P53 negatively slows the cell cycle's advancement and results in apoptosis (Green & Kroemer, 2009).

Cas3 is a protein which is essential for both the intrinsic and extrinsic apoptosis pathways, where activation of members of caspase family caused deterioration of cell structure and function, resulting in cell apoptosis. Moreover, Bcl-2 exhibits anti-apoptotic activity via procaspase sequestration and caspase self-cleavage inhibition (Marsden *et al*., 2002). The obtained immunohistochemical findings coincided with those previously reported from different experimental studies (Abdeen *et al*., 2020; Habib *et al.,* 2021; Eid & Shitany, 2021).

Nevertheless, a significant raise in the immunoreactivity of CD163 protein was recorded in the liver tissues of rats intoxicated with TXL. CD163 is a macrophage-specific protein regulated by various inflammatory mediators, which is switched to alternative activated phenotypes in inflammation via the upregulated expression. It plays an important role in the regulation of immune reactions, as its elevated expression indicates the responding capacity of tissues to inflammation (Skytthe *et al.,* 2020). Moreover, CD163 is regarded as a marker for the detection of activated Kupffer cells as its elevated immunoexpression correlated with increased number of Kupffer cells (Liu *et al*., 2020). The current results are paralleled with those declared by Svendsen *et al*. (2017) after the application of dexamethasone.

The present investigation showed remarkable ultrastructural abnormalities of most organelles of the hepatic cells obtained from TXL-treated animals, including the endoplasmic reticula, mitochondria, lysosomes, and nuclei. The rough endoplasmic reticulum appeared markedly fragmented into small rods, detached from the nucleus, and lost their attached ribosomes. This observation agreed with that of Lushnikova *et al*. (2011) post cyclophosphamide treatment. Also, Focaccetti *et al.* (2015) illustrated marked deterioration of the endoplasmic reticulum following injection with 5-Fluorouracil, as well as Kandil *et al*. (2021) recorded damaged and fragmented cisternae of rough endoplasmic reticulum which lost their attached ribosomes after doxorubicin toxication.

In the current study mitochondria severely altered, lost their cristae and matrices and containing tiny flocculent densities. These results are in line with those of Ahmed and Ghobara (2013) following cisplatin application, Focaccetti *et al*. (2015) post 5-fluorouracil administration, and Kandil *et al.* (2021) after cyclophosphamide treatment.

The fine structural observations of TXL-treated rats` hepatocytes revealed the presence of numerous lysosomes which might be participated in focal cytoplasmic degradation and in the storage or metabolism of such cytotoxic drug. In this regard, the results agreed with those obtained from Ahmed & Ghobara (2013) and Kandil *et al*. (2021). Also, cytoplasmic vacuolization observed in hepatocytes of TXL-treated rats could be resulted from the disruption of the liver cell's ionic equilibrium. Additionally, the buildup of ions and fluids in the cytosol would quickly travel through the permeable membranes of the cell's vacuolated organelles, ultimately resulting in cell lysis (Cheville, 2009). Following TXL-intoxication, the nuclei of hepatocytes showed signs of pyknosis and Karyorrhexis which resulted from the drug's potent DNA binding that contributed to dramatic changes in gene expression. These results are paralleled with those recorded by Kandil *et al.* (2021).

Increased number of activated hypertrophied Kupffer cells, which is recorded as an adverse response of the hepatocytes to TXL cytotoxicity, was a common ultrastructural observation in the current investigation. These activated Kupffer cells had deteriorated cytoplasm and malformed nuclei having electron-dense chromatin materials, as well as extended filopodia. The present findings are alongside with previous investigations carried out by Kamble & Bhiwgade (2011) and Kandil *et al*. (2021).

The disruption in microtubule dynamics, a typical TXL mechanism of action, resulted in interruption of the redox signaling, which can stimulate NADPH oxidase activation and intracellular reactive oxygen species generation. Besides, TXL can directly influence free radical production and polarization of mitochondrial membranes (Ramanathan *et al.*, 2005).

Additionally, TXL has also been reported to rise hydroperoxide output causing oxidative stress in human cancer cells (Alexandre *et al.*, 2006, 2007) which could be the reason for its cytotoxic impact against non-targeted tissues, causing aggregation of peroxides, which is the early and pragmatic step in TXL-induced apoptosis in cancer cells (Alexandre *et al.* 2007). Furthermore, Hadzic *et al.* (2010) declared that TXL elevated the levels of hydrogen peroxide, nitric oxide, and oxidative DNA adducts in breast cancer cell.

Interestingly, concomitant administration of MLT with TXL attenuated the severity of the histological, histomorphometrical and ultrastructural changes in liver tissues of rats treated with TXL. Also, supplementation of MLT to rats subjected to TXL modulated the immunohistochemical expression of the examined reactive proteins; Bcl-2, P53, Cas3, and CD163. The present results are in line with those manifested by Shokrzadeh *et al.* (2014), Barangi *et al.* (2020) and Mi & Kuang (2021).

MLT is one of the body's most potent antioxidants, and research by Zhang *et al.* (2017) has shown that it is essential for controlling liver inflammation and autophagy. Several reports introduced by many authors announced new properties of MLT contributing it as a promising substance that can be used as an adjuvant to chemotherapy and radiotherapy or to be participated with other anti-cancer medication in cancer treatment regimens. The antioxidant activities of MLT are among its most remarkable traits, moreover it has an amphiphilic characteristic, unlike other antioxidants which are either lipophilic or hydrophilic, it can cross physiological boundaries, decreasing oxidative damage in both lipid and aqueous cell environments (Reiter *et al*., 2017; Alonso-González *et al*., 2016, 2018).

Furthermore, Sun *et al.* (2002) reported antiapoptotic characteristics of MLT by enhancing induction of Bcl-2 and capacity in rats following ischemic neuronal injury. MLT has been shown to affect the antioxidant function of Bcl-2 and more commonly against oxidative stress-related deficiencies, paving the way for the therapy of age-induced neural procedures.

Based on the existing histological, histomorphometrical, immunohistochemical, and ultrastructural results, this study manifested that MLT attenuated most of the adverse effects caused by TXL in the liver tissues of adult rats.

Conclusion

The present investigation proved that MLT supplementation into rats has a potential modulating influence against TXL-induced hepatic toxicity through its antioxidant, anti-inflammatory and anti-apoptotic activities. Therefore it is recommended to utilize MLT as a supportive agent to prevent unexpected injury in the liver through chemotherapeutic treatment.

REFERENCES

Abdeen, A.; Abdelkader, A.; Elgazzard, D.; Aboubakre, M.; Abdulahf, O.A., et al. (2020). Coenzyme Q10 supplementation mitigates piroxicam-induced oxidative injury and apoptotic pathways in the stomach, liver, and kidney. Biomed. Pharmacother., 130:1-11.

Ahmed, H.A. and Ghobara, M.M. (2013). Histological study of the effect of cisplatin on the liver of adult male albino rat. Int. J. Acad. Res., 1(1): 22-33.

Alexandre, J.; Batteux, F.; Nicco, C.; Chéreau, C.; Laurent, A.; Guillevin, L., et al. (2006). Accumulation of hydrogen peroxide is an early and crucial step for paclitaxel-induced cancer cell death both in vitro and in vivo. Int. J. Cancer, 119(1):41-48.

Alexandre, J.; Hu, Y.; Lu, W.; Pelicano, H., and Huang, P. (2007). Novel action of paclitaxel against cancer cells: bystander effect mediated by reactive oxygen species. Cancer Res., 67(8): 3512-3417.

Alonso-González, C.; González, A.; Martínez-Campa, C.; Menendez-Menendez, J.; Gomez-Arozamena, J. and Garcia-Vidal, A. (2016). Melatonin enhancement of the radiosensitivity of human breast cancer cells is associated with the modulation of proteins involved in estrogen biosynthesis. Cancer Lett., 370(1):145–152.

Alonso-González, C.; Menéndez-Menéndez, J.; González-González, A.; González, A.; Cos, S. and Martínez-Campa, C. (2018). Melatonin enhances the apoptotic effects and modulates the changes in gene expression induced by docetaxel in MCF-7 human breast cancer cells. Int. J. Oncol., 52(2): 560–570.

Bancroft, J. and Gamble, M. (2002). Theory and practice of histological techniques, Fourth edition, London, Edinburgh, New York, Philadelphia, St. Louis Sydney Toronto.

Barangi, S.; Mehri, S.; Moosavi, Z.; Hayesd, A.W.; Reiter, R.J., et al. (2020). Melatonin inhibits Benzo(a) pyrene induced apoptosis through activation of the Mir-34a/ Sirt1/ autophagy pathway in mouse liver. Ecotoxicol. Environ. Saf., 15(196):1-10.

Bray, F.; Ferlay, J.; Soerjomataram, I.; Siegel, R.L.; Torre, L.A., et al. (2018). Global cancer statistics: GLOBOCAN estimates of incidence and mortality worldwide for 36 cancers in 185 countries. CA Cancer J. Clin., 68(6): 394-424.

Chaudhary, D.; Khatiwada, S.; Sah, S.K., Tamang, M.K., Bhattacharya, S., et al. (2016). Effect of doxorubicin on histomorphology of liver of Wistar albino rats. J. Pharm. Pharmacol., 4: 186-190.

Chen, L.Y.; Tiong, C.; Tsai, C.H.; Liao, W.C.; Yang, S.F.; Youn, S.C., et al. (2015). Early-life sleep deprivation persistently depresses melatonin production and bio-energetics of the pineal gland: potential implications for the development of metabolic deficiency. Brain Struct. Funct., 220(2): 663–676.

Cheville, N.F. (2009). Ultrastructural Pathology. The comparative cellular basis of disease, second edition, Wiley-Blackwell.

Chok, K.C.; Ng, C.H.; Koh, R.Y.; Ng, K.Y. and Chye, S.M. (2019). The potential therapeutic actions of melatonin in colorectal cancer. Horm. Mol. Biol. Clin. Invest. 39(1).

Dana, P.M.; Sadoughi, F.; Mobini, M.; Shafabakhsh, R.; Chaichian, S.; Moazzami, B.; Chamani, M. and Asemi, Z. (2020). Molecular and biological functions of melatonin in endometrial cancer. Curr. Drug Targets, 21: 519–526.

Del Monte, U. (2005). Swelling of hepatocytes injured by oxidative stress suggests pathological changes related to macromolecular crowding. Med. Hypotheses, 64(4): 818–825.

Dykstra, M.J., Mann, P.C., Elwell, M.R. and Ching, S.V. (2002). Suggested standard operating procedures (SOPs) for the preparation of electron microscopy samples for toxicology/ pathology studies in a GLP environment. Toxicol. Pathol., 30(6): 735-743.

Eid, B.G. and Shitany, N.A. (2021). Captopril downregulates expression of Bax / cytochrome C / caspase-3 apoptotic pathway, reduces inflammation, and oxidative stress in cisplatin-induced acute hepatic injury. Biomed. Pharmacother., 139:1-10.

Focaccetti, C.; Bruno, A.; Magnani, E.; Bartolini, D.; Principi, E.; Dallaglio, K.; et al. (2015). Effects of 5-Fluorouracil on morphology, cell cycle, proliferation, apoptosis, autophagy and ROS production in endothelial cells and cardiomyocytes. PLoS One, 10(2): 1-25.

Fürst, R. and Vollmar, A.M. (2013). A new perspective on old drugs: non-mitotic actions of tubulin-binding drugs play a major role in cancer treatment. Pharmazie, 68(7): 478–483.

Ghafouri-Fard, S.; Shoorei, H.; Abak, A.; Seify, M.; Mohaqiq, M., et al. (2021). Effects of chemo-therapeutic agents on male germ cells and possible ameliorating impact of antioxidants. Biomed. Pharmacother., 142:1-21.

Ghasemi, F.M., Faghani, M., Khajehjahrom, S., Bahadori, M.; Nasiri, E.; and Hemadi, M. (2010). Effect of Melatonin on Proliferative Activity and Apoptosis in Spermatogenic Cells in Mouse under Chemotherapy. J. Rep. Contrac., 21(2): 79-94.

Green, D.R. and Kroemer, G. (2009). Cytoplasmic functions of the tumor suppressor p53. Nature, 458(7242):1127–1130.

Habib, S.A.; Suddek, G.M.; Abdel-Rahim, M. and Abdelrahman, R.S. (2021). The protective effect of protocatechuic acid on hepatotoxicity induced by cisplatin in mice. Life Sci., 277:1-15.

Hadzic, T.; Aykin-Burns, N.; Zhu, Y.; Coleman, M.C.; Leick, K., Jacobson, G.M., and Spitz, D.R. (2010). Paclitaxel combined with inhibitors of glucose and hydroperoxide metabolism enhances breast cancer cell killing via H_2O_2-mediated oxidative stress. Free Radic. Biol. Med., 48(8): 1024-1039.

Hardeland, R.; Cardinali, D.P.; Srinivasan, V., Spence, D.W., Brown, G.M., and Pandi-Perumal, S.R. (2011). Melatonin- A pleiotropic, orchestrating regulator molecule. Progress in Neurobiol., 93(3): 350-84.

Hardin, C.; Shum, E.; Singh, A.P., Perez-Soler, R. and Cheng, H. (2017). Emerging treatment using tubulin inhibitors in advanced non-small cell lung cancer. Expert. Opin. Pharm.,18(7): 701–716.

Hashish, E.A. and Elgaml, S.H. (2016). Protective effect of melatonin against chromium induced hepato- toxic and genotoxic effect in albino rats. Global Veterin., 16(4): 323-329.

Hassan, H.M.; Al-Wahaibi, L.H.; Elmorsy, M.A. and Mahran, Y.F. (2021). Suppression of cisplatin-induced hepatic injury in rats through alarmin high - mobility group Box-1 pathway by ganoderma - lucidum: theoretical and experimental study. Drug Des. Devel. Ther., 14: 2335–2353.

Heinig, U.; Scholz, S. and Jennewein, S. (2013). Getting to the bottom of Taxol biosynthesis by fungi. Fungal Divers, 60: 161-70.

Huang, C.Y.; Cheng, M.; Lee, N.R.; Huang, H.Y.; Lee, W.L., et al. (2020). Comparing paclitaxel-carboplatin with paclitaxel-cisplatin as the front-line chemotherapy for patients with FIGO IIIC serous-type tubo-ovarian cancer. Int. J. Environ. Res. Public Health, 17(7): 2213.

Johar, D.; Roth, J.C.; Bay, G.H.; Walker, J.N.; Kroczak, T.J. and Los, M. (2004). Inflammatory response, reactive oxygen species, programmed (necrotic-like and apoptotic) cell death and cancer. Roczniki Akademii Medycznej W Białymstoku, 49: 31–39.

Kamble, P.R. and Bhiwgade, D.A. (2011). Cisplatin induced histological and ultrastructural alterations in liver tissue of rat. J. Cytol. Histol., 2(6): 1-5.

Kandil, E.H.; Okdah, Y.A. and Moselhy, A.G. (2021). Effect of thyme oil on doxorubicin - induced hepatotoxicity in female albino rats: histological, ultrastructural, and biochemical studies. E.J.Z., 76(76): 76-90.

Khorwal, G.; Chauhan, R. and Nagar, M. (2017). Effect of cyclophosphamide on liver in albino rats: a comparative dose dependent histo-morphological study. Int. J. Biomed. Adv. Res., 8(03): 102-107.

Kiernan, J.A. (2015). Histological and Histochemical Methods: Theory and practice, Fourth edition, Scion Publishing Ltd, pp. 454-548.

Kong, X.; Gao, R.; Wang, Z.; Wang, X.; Fang, Y.; Gao, J., et al. (2020). Melatonin: a potential therapeutic option for breast Cancer, Trends Endocrinol. Metab., 31: 859–871.

Lemstrova, R.; Melichar, B. and Mohelnikova - Duchonova, B. (2016). Therapeutic potential of taxanes in the treatment of metastatic pancreatic cancer. Cancer Chemother. Pharm., 78(6): 1101–1111.

Liu, Y.; Tian, F.; Shan, J., Gao, J.; Li, B.; Lv, J.; Zhou, X.; Cai, X.; Wen, H. and Ma, X. (2020). Kupffer cells: important participant of hepatic alveolar Echinococcosis. Echinococcosis. Front. Cell Infect. Microbiol., 10(8):1-9.

Luo, C.; Yang, Q.; Liu, Y.; Zhou, S.; Jiang, J.; Reiter, R.J.; Bhattachary, P., et al. (2019). The multiple protective roles and molecular mechanisms of melatonin and its precursor N-acetylserotonin in targeting brain injury and liver damage and in maintaining bone health. Free Radical Biol. Med., 130: 215–33.

Lushnikova, E.L.; Molodykh, O.P.; Nepomnyashchikh, L.M.; Bakulina, A.A. and Sorokina, Y.A. (2011). Ultrastructural picture of cyclophosphamide - induced damage to the liver. Bull. Exp. Biol. Med., 151(6): 751- 756.

Maleki, D.P.; Reiter, R.J.; Hallajzadeh, J.; Asemi, Z.; Mansournia, M.A. and Yousefi, B. (2020). Melatonin as a potential inhibitor of kidney cancer: a survey of the molecular processes, IUBMB Life, 72(11): 2355–2365.

Malekinejad, H.; Ahsan, S.; Delkhosh-Kasmaie, F.; Cheraghi, H.; Rezaei-Golmisheh, A. and Janbaz-Acyabar, H. (2015). Cardioprotective effect of royal jelly on paclitaxel-induced cardiotoxicity in rats. Iran J. Basic Med. Sci., 19: 221-27.

Malekinejad, H.; Fani, M.; Shafiee-Roodbari, S.K.H., Delkhosh-Kasmaie, F., and Rezaei - Golmisheh, A. (2017). Crosstalk between E2f1 and c-Myc mediates hepato-protective effect of royal jelly on taxol-induced damages. Human Exper. Toxicol., 36(6): 626–37.

Marsden, V.S.; O'connor, L.; O'reilly, L.A., Silke, J., Metcalf, D., et al. (2002). Apoptosis initiated by Bcl-2-regulated caspase activation independently of the cytochrome c/Apaf-1/caspase-9 apoptosome. Nature, 419(6907): 634–637.

Marupudi, N.I.; Han, J.E. and Li, K.W. (2007). Paclitaxel: a review of adverse toxicities and novel delivery strategies. Exper. Opin. Drug Saf., 6: 609-621.

Mehrzadi, M.H.; Hosseinzadeh, A.; Juybari, K.B. and Mehrzadi, S. (2020). Melatonin and urological cancers: a new therapeutic approach. Cancer Cell Int., 10(20):444.

Mi, L. and Kuang, H. (2021). Melatonin regulates cisplatin resistance and glucose metabolism through hippo signaling in hepatocellular carcinoma cells. Cancer Manag. Res.,12: 1863–1874.

Oshiba, R.T.; Touson, E.; Elsherbini, Y.M. and Abdraboh, M.E. (2021). Melatonin: a regulator of the interplay between FoxO1, miR96, and miR215 signaling to diminish the growth, survival, and metastasis of murine adenocarcinoma, BioFactors, 47: 740–753.

Ozcelik, B.; Turkyilmaz, C.; Ozgun, M.T.; Serin, I.S.; Batukan, C., Ozdamar, S., and Ozturk, A.

(2010). Prevention of paclitaxel and cisplatin induced ovarian damage in rats by a gonadotropin-releasing hormone agonist. Fertil Steril., 93: 1609–1614.

Ozougwu, J.C. (2017). Physiology of the liver. Int. J. Res. Pharm. Biosci., 4(8): 13-24.

Palipoch, S.; Punsawad, C.; Koomhin, P. and Suwannalert, P. (2014). Hepatoprotective effect of curcumin and alpha-tocopherol against cisplatin induced oxidative stress. BMC. Complement. Altern. Med., 14:111.

Plaimee, P.; Khamphio, M.; Weerapreeyakul, N.; Barusrux, S., and Johns, N.P. (2014). Immuno-modulatory effect of melatonin in SK-LU-1 human lung adeno-carcinoma cells co-cultured with peripheral blood mono-nuclear cells, Cell Prolif., 47: 406–415.

Pourhanifeh, M.H., Kamali, M., Mehrzadi, S. and Hosseinzadeh, A. (2021). Melatonin and neuro-blastoma: a novel therapeutic approach. Mol. Biol. Rep., 48: 4659–4665.

Ramanathan, B.; Jan, K.Y.; Chen, C.H.; Hour, T.C.; Yu, H.J. and Pu, Y.S. (2005). Resistance to paclitaxel is proportional to cellular total antioxidant capacity. Cancer Res., 65(18): 8455-8460.

Reiter, R.J.; Rosales-Corral, S.; Tan, D.X.; Jou, M.J.; Galano, A. and Xu, B. (2017). Melatonin as a mitochondria - targeted antioxidant: one of evolution's best ideas. Cell Mol. Life Sci, 74: 3863–3881.

Ren, W.; Liu, G.; Chen, S.; Yin, J.; Wang, J.; Tan, B.; Wu, G., et al. (2017). Melatonin signaling in T cells: functions and applications. J. Pineal Res., 62(3): 1-15.

Samei, E.; Mozdarani, H.; Samiei, F. and Javadi, G. (2021). Radioprotective effects of combined melatonin and famotidine treatment on radiation induced apoptosis in peripheral blood leukocytes of breast cancer patients and Normal individuals. Cell J., 23: 562–567.

Sato, K.; Hall, C.; Glaser, S.; Francis, H.; Meng, F., et al. (2016). Pathogenesis of Kupffer cells in cholestatic liver injury. Am. J. Pathol., 186(5): 2238- 2247.

Serizawa, K.; Yogo, K.; Aizawa, K.; Tashiro, Y.; Takahari, Y.; Sekine, K., et al. (2012). Paclitaxel-induced endothelial dysfunction in living rats is prevented by nicorandil via reduction of oxidative stress. J. Pharmacol. Sci., 119(4): 349–358.

Shokrzadeh, M.; Ahmadi. A.; Naghshvar. F.; Chabra. A. and Jafarinejhad, M. (2014). Prophylactic efficacy of melatonin on cyclo-phosphamide-induced liver toxicity. Biomed. Res. Int., 2014:1-6.

Skytthe, M.K.; Graversen, J.H. and Moestrup, S.K. (2020). Targeting of CD163+ macrophages in inflammatory and malignant diseases. Int. J. Mol. Sci., 21(15): 5497.

Smith, E.R.; Leal, J.; Amaya, C.; Li, B. and Xu, X.X. (2021). Nuclear lamin A/C expression is a key determinant of paclitaxel sensitivity. Mol. Cell Biol., 41(7): e0064820.

Smith, E.R. and Xu, X.X. (2021). Breaking malignant nuclei as a non-mitotic mechanism of taxol/ paclitaxel. J. Cancer Biol., 2(4): 86–93.

Sun, F.Y.; Lin, X.; Mao, L.Z.; Ge, W.H., Zhang, L.M., Huang, Y.L., and Gu, J. (2002). Neuroprotection by melatonin against ischemic neuronal injury associated with modulation of DNA damage and repair in the rat following a transient cerebral ischemia. J Pineal Res., 33:48–56.

Svendsen, P.; Graversen, J.H.; Etzerodt, A.; Hager, H.; Roge, R., et al. (2017). Antibody-directed glucocorticoid targeting to CD163 in M2-type macrophages attenuates fructose-induced liver inflammatory changes. Mol. Ther. Methods Clin. Dev., 4: 50-61.

Tamtaji, O.R.; Mirhosseini, N.; Reiter, R.J.; Behnamfar, M. and Asemi, Z. (2019). Melatonin and pancreatic cancer: current knowledge and future perspectives, J. Cell. Physiol., 234: 5372–5378.

Tzifi, F.; Economopoulou, C.; Gourgiotis, D.; Ardavanis, A.; Papageorgiou, S., et al. (2012). The role of BCL2 family of apoptosis regulator proteins in acute and chronic leukemias. Adv. Hematol., 1-15.

Yang, C.H. and Horwitz, S.B. (2017). Taxol®: the first microtubule stabilizing agent. Int. J. Mol. Sci., 18(8): 1733.

Yu, X., Li, Z., Zheng, H., Ho, J., Chan, M.T., and Wu, W.K. (2016). Protective roles of melatonin in central nervous system diseases by regulation of neural stem cells. Cell Proliferation, 50(2): 1-5.

Zhang, J.J.; Meng, X.; Li, Y.; Zhou, Y.; Xu, D.P.; Li, S., and Li, H.B. (2017). Effects of melatonin on liver injuries and diseases. Int. J. Mol. Sci., 18 (4): 673.

The ameliorative influence of melatonin against hepatotoxicity-induced by taxol in adult rats

التأثير التحسيني للميلاتونين ضد السمية الكبدية التي يسببها التاكسول فى الجرذان البالغة

هناء رزق أبوالوفا أحمد* ، رمضان عبد الصادق رمضان ، فاتن محمد عبدالحميد

قسم العلوم البيولوجية والجيولوجية – كلية التربية – جامعة عين شمس

المستخلص

على الصعيد العالمي، يعتبر السرطان مشكلة صحية متنامية تسببت في التوسع في استخدام العلاج الكيميائي الذي لا يزال الطريقة الأكثر شيوعًا والخط الأول لعلاج الأورام الخبيثة. هدفت الدراسة الحالية الي استخدام بروتوكولات علم الأنسجة والقياسات المورفوميترية النسيجية والكيميائية المناعية النسيجية والتركيبة الدقيقة لتقييم التأثير السمي للكبد من عقار تاكسول (TXL) والتأثير التحسيني للميلاتونين (MLT) ضد التأثيرات السامة في كبد الجرذان البالغة. تم توزيع خمسين جرذا بشكل عشوائي إلى أربع مجموعات: المجموعة الضابطة ، مجموعة الشام ، مجموعه التاكسول (٧.٥ مجم /كجم عن طريق التجويف البريتوني) ، مجموعة الميلاتونين (١٠ مجم /كجم عن طريق التجويف البريتوني) ومجموعة الميلاتونين + التاكسول (١٠ مجم/ كجم + ٧.٥ مجم/ كجم عن طريق التجويف البريتوني). تم الكشف عن العديد من التغييرات النسيجية المرضية، القياسات المورفوميترية النسيجية ، والتغيرات التركيبية الدقيقة في الأنسجة الكبدية للحيوانات المعالجة بـالتاكسول متضمنة تدمير البناء الطبيعي للفصصيصات الكبدية ، مع انخفاض ملحوظ في عدد خلايا الكبدية السليمة ، وزيادة في عدد الخلايا الكبدية النخرية ، والخلايا الالتهابية في المنطقة الفصية المركزية والمحيطة البابية ، وخلايا كوبفر المتدهورة ، بالإضافة إلى موت الخلايا المبرمج الملحوظ الذي تم تمثيله مناعيًا بارتفاع ملحوظ في P53 و Cas3 ، ونقص في نشاط مناعة Bcl2. أيضًا ، لوحظ نشاط مناعي قوي لـ CD163 في الجرذان المعالجة بـالتاكسول. في حين أن المعالجة المتزامنة بالميلاتونين مع التاكسول عكست معظم التغييرات النسيجية والتركيبية الدقيقة التي سببها التاكسول في الجرذان. بالإضافة إلى ذلك ، كشف الميلاتونين عن تأثير متناقص ضد موت الخلايا المبرمج في الكبد والالتهاب الناجم عن التاكسول والذي تمثل بارتفاعًا في التعبير المناعي لـ Bcl-2 وانخفاض التعبير المناعي لـ P53 و Cas3 و CD163. أثبتت الدراسة الحالية أن الميلاتونين له تأثير محسن ضد السمية الكبدية التي سببها التاكسول من خلال خصائصها المضادة للأكسدة والمضادة للالتهابات والمضادة لموت الخلايا المبرمج.